

A NUMERICAL STUDY OF A PATHOLOGICAL EXAMPLE OF p-SYSTEM*

PHILIPPE HOCH[†] AND MICHEL RASCLE[†]

Abstract. In this paper, we consider several high-order schemes in one space dimension. In particular, we compare the second-order relaxation ($\epsilon \ll 1$) or “relaxed” ($\epsilon = 0$) schemes of Jin and Xin [*Comm. Pure Appl. Math.*, 48 (1995), pp. 235–277] with the second-order Lax–Friedrichs scheme of Nessyahu and Tadmor [*J. Comp. Phys.*, 87 (1990), pp. 408–463] and with higher-order essentially nonoscillatory (ENO) and weighted essentially nonoscillatory (WENO) schemes. This comparison is made first on a Sod shock tube and then on a very pathological example of a p-system constructed by Greenberg and Rascle [*Arch. Ration. Mech. Anal.*, 115 (1991), pp. 395–407]. This exotic system admits a family of periodic solutions which are shock-free but present pairs of *interacting centered compression waves*. Therefore, the exact solution contains big spikes. We show how these different schemes face this numerical challenge.

Key words. systems of conservation laws, high order schemes, second order relaxation and Lax–Friedrichs schemes

AMS subject classifications. 35L65, 35L67, 65M06

PII. S0036142997323181

1. Introduction. The motivation of this paper was to compare several second- or higher-order schemes—which are described precisely below—on a couple of mono-dimensional problems. The first example is of course the Sod shock tube. The second case is a pathological example of a p-system constructed in [1]; see also [2]. This system is built with a very specific pressure law (see the details in section 2) and admits a family of periodic solutions in space and time. In particular, those solutions are shock-free but present centered compression waves which interact and produce severe spikes. Although this problem is one-dimensional, we have thought it would be interesting to use it as a challenging case to compare several second- or higher-order finite volume schemes. Namely, we have considered the second-order relaxation ($\epsilon \ll 1$) or relaxed ($\epsilon = 0$) schemes of Jin–Xin [4]. We have compared these schemes on one hand with the staggered second-order Lax–Friedrichs scheme of Nessyahu–Tadmor [6] and on the other hand with higher-order essentially nonoscillatory (ENO) and weighted essentially nonoscillatory (WENO) schemes, first on Sod’s shock tube for Euler equations and then on this pathological p-system. Not surprisingly, all these schemes work rather well, even in the second case, where the exact solution itself presents big spikes due to the interaction of centered compression waves.

The outline of the paper is as follows. In section 2, we briefly recall the description of this exotic example constructed in [1]. In sections 3 and 4, we recall a few basic facts, first on higher finite volume schemes and then on second-order relaxation schemes. In section 5, we first compare all these schemes on the more classical—and in practice, more useful!—example of Sod’s shock tube, and then we present our numerical results and comments on this pathological example, in particular on the presence of spikes, before a brief conclusion in section 6.

*Received by the editors June 16, 1997; accepted for publication (in revised form) October 14, 1998; published electronically September 8, 1999.

<http://www.siam.org/journals/sinum/36-5/32318.html>

[†]Laboratoire de Mathématiques, U.M.R CNRS No. 6621, Université de Nice, Parc Valrose B.P. 71, F06108 Nice Cédex 2, France (hoch@math.unice.fr, rascle@math.unice.fr).

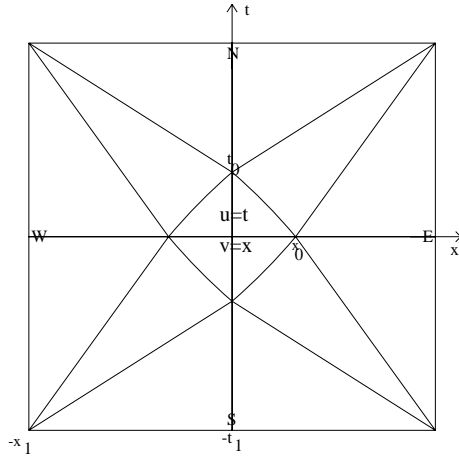


FIG. 2.1.

2. A pathological example of p -system. We consider here the p -system, or more exactly the system of one-dimensional nonlinear elasticity in Lagrangian coordinates

$$(2.1) \quad \begin{cases} \partial_t u - \partial_x v = 0, \\ \partial_t v - \partial_x \sigma(u) = 0, \end{cases}$$

where u denotes the strain, $\sigma = \sigma(u)$ the stress, and v the velocity.

In a very particular case where $\sigma(\cdot)$ is an odd function, Greenberg and Rascle [1] have constructed a sequence of periodic solutions in time and space, $(u^\epsilon, v^\epsilon)(x, t) := (u, v)(\frac{x}{\epsilon}, \frac{t}{\epsilon}), \epsilon \searrow 0$, which satisfies the following properties:

The function u (resp., v) is odd (resp., even) in x and even (resp., odd) in t . Moreover (see Figure 2.1), the basic pattern is the interaction of two centered rarefaction waves between two constant states N, S (north, south),

$$N := \begin{pmatrix} u = t_0 \\ v = 0 \end{pmatrix}, \quad S := \begin{pmatrix} u = -t_0 \\ v = 0 \end{pmatrix}, \quad t_0 > 0,$$

and involves two other constant states E, W (east, west),

$$E := \begin{pmatrix} u = 0 \\ v = x_0 \end{pmatrix}, \quad W := \begin{pmatrix} u = 0 \\ v = -x_0 \end{pmatrix}, \quad x_0 > 0.$$

In the interior domain of central interaction, the solution is supposed to be the universal solution $(u, v) \equiv (t, x)$. The law is chosen so that the interaction of these two centered rarefaction waves converts them into centered compressive waves and not into shocks, which would consume energy and would prevent the solution from being periodic in time. In order to obtain this pattern, the constitutive relation σ must satisfy an ODE whose solution is written as

$$\sigma(u) = \frac{c_0^2 \lambda^4}{3} \operatorname{sgn}(u) \left(\frac{1}{(\lambda - |u|)^3} - \frac{1}{\lambda^3} \right), \quad \lambda = t_1 > t_0.$$

In particular, σ is such that

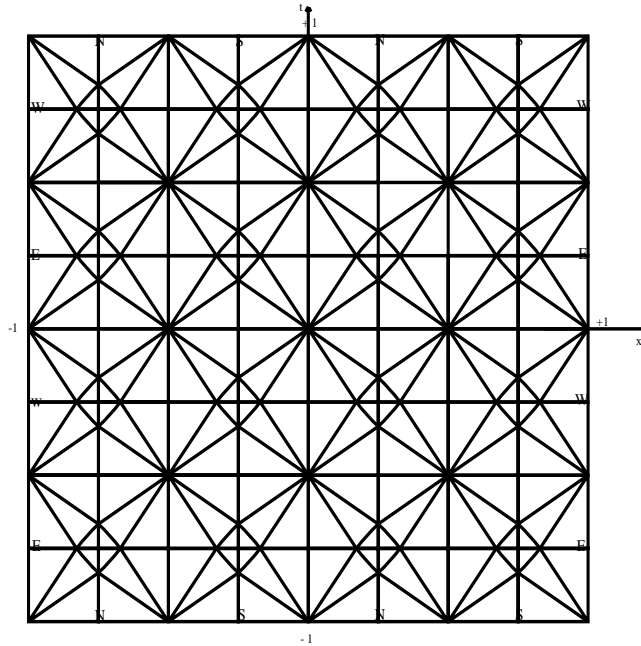


FIG. 2.2.

1. $\forall u \neq 0, u\sigma''(u) > 0, \sigma$: odd. The system is genuinely nonlinear, except for $u = 0$, at which σ presents an inflection point; cf. section 5, Figure 5.5.
2. σ is of class C^2 , except at $u = 0$, where it is only C^1 .

It is important to notice that if σ were smooth at $u = 0$, then, following Di Perna's result [12], $\forall t > 0$, the initial oscillations of the sequence (u^ϵ, v^ϵ) would be canceled by the nonlinear interactions. Therefore, the sequence (u^ϵ, v^ϵ) considered here is very pathological, since large amplitude oscillations persist, although no eigenvalue is linearly degenerate. In particular, it does not belong to the class of solutions for which Serre [16], [17] constructed formal asymptotic expansions. We have tested a few numerical schemes on this problem with $(x, t) \in (-1, 1)^2$, with $x_1 = t_1 = 1$.

The solution consists of 4×4 basic patterns (see Figure 2.2).¹

The initial data (resp., boundary conditions on $x = -1$ and $x = +1$) on the four successive subintervals are NSNS (resp., EWEW and EWEW).

From the numerical point of view, we remark that this solution has no shock but contains centered rarefaction and compression waves which even interact so that the exact solution presents big spikes, and we also remark that the stress-strain relation σ has an inflection point. These unusual features are therefore a good challenge to test several classical second-(or higher-) order numerical schemes. Before describing the numerical results in section 5, we first must describe the schemes we have used.

3. Basic facts on high-order finite volume schemes. We consider the initial value problem for a general one-dimensional system of N conservation laws:

$$(3.1) \quad \partial_t U + \partial_x F(U) = 0,$$

¹More exactly, we should consider that a basic pattern is in fact *four* adjacent patterns (see Figure 2.1), in order to recover the same constant states at the boundary of the period.

$$(3.2) \quad U(x, 0) = U_0(x).$$

The system is supposed strictly hyperbolic. We denote by R the matrix of right eigenvectors $r_k(U)$ of $F'(U)$ and we set $L := R^{-1}$. We briefly recall the classical construction of high-order finite volume schemes: Let \bar{U}_j^n denote the average value of the numerical solution $U(\cdot, t)$ on the cell $C_j =]x_{j-\frac{1}{2}}, x_{j+\frac{1}{2}}[$ computed at time t^n . Here, we have set $x_j = x_0 + j\Delta x$.

After integration of (3.1) over the rectangle $C_j \times (t^n, t^{n+1})$, we have to find an approximation of

$$(3.3) \quad \bar{U}_j^{n+1} = \bar{U}_j^n - \lambda \left(F_{j+\frac{1}{2}} - F_{j-\frac{1}{2}} \right),$$

where $F_{j+\frac{1}{2}} = \frac{1}{\Delta t} \int_{t^n}^{t^{n+1}} F(U(x_{j+\frac{1}{2}}, t)) dt$, and $\lambda = \Delta t / \Delta x$.

Following Harten et al. [8], we split the algorithm into three steps: reconstruction, evolution, and averaging. In the reconstruction step, which we will recall below, we start with the averages \bar{U}_j^n to construct a new function $R(x, \bar{U})$ polynomial on each cell. In the evolution step, we now consider the initial value problem

$$(3.4) \quad \begin{aligned} \partial_t W + \partial_x F(W) &= 0, & t \in (t^n, t^{n+1}), \\ W(x, t^n) &= R(x, \bar{U}^n). \end{aligned}$$

The question is how to approximate the integral

$$I = \frac{1}{\Delta t} \int_{t^n}^{t^{n+1}} F(W(x_{j+\frac{1}{2}}, t)) dt.$$

If the function $t \mapsto F(W(x_{j+\frac{1}{2}}, t))$ were known, we would of course use a Gauss-type formula of order r :

$$I \simeq \sum_{k=1}^s \alpha_k F(W(x_{j+\frac{1}{2}}, t^n + \beta_k \Delta t)) + O(\Delta t^r).$$

For instance, typical choices are

1. order 1: $s = 1$, $\alpha_1 = 1$, and $\beta_1 = 0$,
2. order 2: $s = 1$, $\alpha_1 = 1$, and $\beta_1 = \frac{1}{2}$,
3. order 4: $s = 2$, $\alpha_1 = \alpha_2 = \frac{1}{2}$, $\beta_1 = \frac{1}{2}(1 - \frac{\sqrt{3}}{3})$, $\beta_2 = \frac{1}{2}(1 + \frac{\sqrt{3}}{3})$.

Now, in order to approximate the above function $F(W((x_{j+\frac{1}{2}}, \cdot)))$, we consider the local Riemann problem:

$$(3.5) \quad \begin{aligned} \partial_t Z + \partial_x F(Z) &= 0, \\ Z(x, 0) &= \begin{cases} a_{j+\frac{1}{2}}^k, \\ b_{j+\frac{1}{2}}^k, \end{cases} \end{aligned}$$

where $a_{j+\frac{1}{2}}^k$ (resp., $b_{j+\frac{1}{2}}^k$) is constructed in the following way [8]: Starting from polynomial data $v_j(x)(= R_j(x, \bar{U}))$ in the cell C_j , we first extend this initial data to the neighbor cells. The corresponding solution $v_j(x, t)$ is locally smooth, and $a_{j+\frac{1}{2}}^k$ is the value at point $(x_{j+\frac{1}{2}}, t^n + \beta_k \Delta t)$ of the Taylor expansion of $v_j(x, t)$, denoted by $\tilde{v}_j(x, t^n + t)$, around the point (x_j, t^n) , in which we have used the equation to replace all the time derivatives by space derivatives. Of course $b_{j+\frac{1}{2}}^k$ is constructed in a similar

way in the cell C_{j+1} ; therefore, for $i = j, j + 1$ and $r = 3$,

$$a_{j+\frac{1}{2}}^k = \tilde{v}_j(x_{j+\frac{1}{2}}, t^n + \beta_k \Delta t) \quad \text{and} \quad b_{j+\frac{1}{2}}^k = \tilde{v}_{j+1}(x_{j+\frac{1}{2}}, t^n + \beta_k \Delta t),$$

$$\tilde{v}_i(x, t^n + t) = \tilde{v}_i(x, t^n) - t \partial_x f(\tilde{v}_i(x, t^n)) + \frac{t^2}{2} \partial_x (f'(\tilde{v}_i(x, t^n)) \partial_x f(\tilde{v}_i(x, t^n))),$$

with $\tilde{v}_i(x, t^n) = v_i(x, 0) = R(x, \bar{u})|_{C_i}$.

Therefore, with the property on $R(x, \bar{u})$,

$$\frac{d^k}{dx^k} R_i(x, \bar{u}^n) = \frac{\partial^k}{\partial x^k} u(x, t^n + t) + O(\Delta x^{r-k}), \quad 0 \leq k \leq r - 1.$$

We have $\tilde{v}_i(x, t^n + t) = u(x, t^n + t) + O(\Delta x^r)$ when $\Delta x = O(\Delta t)$.

Therefore, the exact flux of the solution to the Riemann problem (3.5) satisfies $f^G(a, b) = f(Z^R(0, a, b)) = f(u(x_{j+\frac{1}{2}}, t^n + t)) + O(\Delta x^r)$, where f^G means the Godunov flux. Practically we may take any numerical flux $g(a, b)$ which is Lipschitz continuous and monotone. Here, we will use the Roe scheme with the entropy fix used by Osher–Shu; see [9]. The averaging is obtained by taking the average value of the solution $U(x, t^{n+1})$ on the cell C_j . Finally, the scheme is written as

$$(3.6) \quad \bar{U}_j^{n+1} = \bar{U}_j^n - \lambda \left(\sum_{k=1}^s \alpha_k (g(a_{j+\frac{1}{2}}^k, b_{j+\frac{1}{2}}^k) - g(a_{j-\frac{1}{2}}^k, b_{j-\frac{1}{2}}^k)) \right).$$

Of course, the Godunov and Van Leer MUSCL schemes belong to this class, as well as the ENO schemes and also the (second-) order staggered Lax–Friedrichs scheme of Nessyahu–Tadmor [6], provided that we average at each time step on the staggered grid. Of course that avoids using any Riemann solver. This scheme can also be viewed as a predictor-corrector scheme:

$$(3.7) \quad \bar{U}_j^{n+\frac{1}{2}} = \bar{U}_j^n - \frac{\lambda}{2} F_j'^n,$$

$$(3.8) \quad \bar{U}_{j+\frac{1}{2}}^{n+1} = \frac{1}{2} (\bar{U}_j^n + \bar{U}_{j+1}^n) - \frac{1}{8} (U_{j+1}'^n - U_j'^n) - \lambda \left(F(\bar{U}_{j+1}^{n+\frac{1}{2}}) - F(\bar{U}_j^{n+\frac{1}{2}}) \right),$$

where $F_j'^n/\Delta x$ and $U_j'^n/\Delta x$ are numerical approximation of, resp., $\partial_x F(U(x_j, t^n))$ and $\partial_x U(x_j, t^n)$.

Now, if Δt goes to zero in (3.6), we obtain

$$(3.9) \quad \frac{d}{dt} \bar{U}_j(t) = -\frac{1}{\Delta x} \left(g(R_j(x_{j+\frac{1}{2}}, \bar{U}), R_{j+1}(x_{j+\frac{1}{2}}, \bar{U})) - g(R_{j-1}(x_{j-\frac{1}{2}}, \bar{U}), R_j(x_{j-\frac{1}{2}}, \bar{U})) \right),$$

which allows us to uncouple spatial and temporal approximations.

Now, (3.9) is a system of ODEs that we approach with the Runge–Kutta total variation diminishing (TVD) method of Osher–Shu [9, pp. 444–447].

As observed in [10], the WENO reconstruction allows us to gain one order of accuracy at the interfaces. Therefore, the time approximation must be of order $(r + 1)$ to exploit this gain.

We now briefly recall the reconstruction procedure. Starting with known averages \bar{U}_j^n on each cell C_j , we construct a piecewise polynomial function $R(x, \bar{U})$ which satisfies the following properties:

- (i) high-order approximation in regions where the solution is smooth: $R_j(x, \bar{U}) = U(x, t) + e(x)\Delta x^r + O(\Delta x^{r+1})$;
- (ii) conservation of average values: $\bar{R}(x_j, \bar{U}) = \bar{U}_j$;
- (iii) control of oscillations, either TVD no oscillation is created: $TV(R(x, \bar{u})) \leq TV(u)$ or ENO: $TV(R(x, \bar{u})) \leq TV(u) + O(\Delta x^r)$.

We begin with the scalar case, in which the construction is based on the primitive of $u(\cdot, t)^2$:

$$W(x) = \int_{x_{j_0 - \frac{1}{2}}}^x u(y, t) dy,$$

with $W(x_{j+\frac{1}{2}}) = \Delta x \sum_{k=j_0}^j \bar{u}_k$. Knowing the values of W at the interfaces provides an approximation of u by evaluating the derivatives of a polynomial interpolation of W at the interfaces. Let us simply recall that we typically obtain

- (i) for $r = 1$, the Godunov scheme: $R_j(x, \bar{u}) = \bar{u}_j$;
- (ii) for $r = 2$, Van Leer's type of schemes: $R_j(x, \bar{u}) = \bar{u}_j + \frac{\sigma_j}{\Delta x}(x - x_j)$, where $\sigma_j = \Delta x \partial_x u(x_j, t) + O(\Delta x^2)$ if TVD or $\sigma_j = \Delta x \partial_x u(x_j, t) + O(\Delta x^3)$ if uniformly nonoscillatory (UNO) (see [7]);
- (iii) for $r > 2$, either the ENO or the WENO type of schemes. The latter involves a convex combination of *all* the interpolation polynomials of W on the stencil $S_{j+k} = (x_{j+k-r+\frac{1}{2}}, \dots, x_{j+k+\frac{1}{2}})$, whereas the former involves only *one* of them.

Finally, in the case of systems considered here, the reconstruction has been performed either componentwise, e.g., in LF2, or in characteristic variables (ENO, WENO). In the next section, we recall the construction of relaxation schemes [4].

4. Second-order relaxation schemes. The basic idea of relaxation schemes [4] is to (formally) consider a nonlinear hyperbolic system of conservation laws,

$$(4.1) \quad \partial_t U + \partial_x F(U) = 0,$$

as the zero-relaxation limit, of a sequence of semilinear hyperbolic systems of size $2N$, with a stiff source term:

$$(4.2) \quad \partial_t U + \partial_x V = 0,$$

$$(4.3) \quad \partial_t V + A^2 \partial_x U = \frac{1}{\epsilon}(F(U) - V), \quad \epsilon \searrow 0.$$

Here A^2 is a constant diagonalizable matrix (practically, A is diagonal), and we assume that the classical subcharacteristic condition of Whitham [15], and Liu [13] is satisfied, namely, that the characteristic speeds of the full system (4.2) (4.3) “dominate” those of the relaxed equilibrium system (4.1) : $A^2 \geq F'(U)^2$; see a more precise statement in [14]. Let $(U, V) := (U^\epsilon, V^\epsilon)$ be the solution to (4.2), (4.3). If we consider the Chapman-Enskog expansion

$$V^\epsilon = V_0(U) + \epsilon V_1(U, \partial_x U) + \dots,$$

where U is the solution to the equilibrium system, then (see, e.g., [18]) we classically obtain

²This is called reconstruction via primitive function.

$$V_0(U) = F(U^\epsilon),$$

and finally, at the order ϵ , U^ϵ satisfies

$$(4.4) \quad \partial_t U^\epsilon + \partial_x F(U^\epsilon) = \epsilon \partial_x ((A^2 - F'(U^\epsilon)^2) \partial_x U^\epsilon),$$

which is well-posed, in view of the subcharacteristic condition. There are essentially two classes of schemes introduced in [4]. In either case, the scheme is based on the obvious splitting between the stiff ODE,

$$(4.5) \quad \begin{cases} \partial_t U = 0, \\ \partial_t V = \frac{1}{\epsilon} (F(U) - V), \end{cases}$$

and the conservation law without source term,

$$(4.6) \quad \begin{cases} \partial_t U + \partial_x V = 0, \\ \partial_t V + A^2 \partial_x U = 0. \end{cases}$$

The stiff ODE (4.5) is either approximated with an implicit (not A-stable) second-order Runge–Kutta method or replaced by the equilibrium relation

$$(4.7) \quad V := F(U).$$

The latter choice is much more natural as soon as the time step satisfies

$$(4.8) \quad \Delta t / \epsilon \gg 1,$$

which is the practical case. As in [4], in order to approximate the convective part (4.6), we use here the MUSCL reconstruction, based on the Riemann invariants. We consider here the case where $A = c I$, $c > 0$, where I is the unit 2×2 matrix. The corresponding vector-valued Riemann invariants are the linear functions

$$(4.9) \quad W = V + AU, \quad Z = V - AU, \quad W, Z \in \mathbb{R}^2,$$

and the subcharacteristic condition is simply

$$(4.10) \quad c^2 \geq \sigma'(u).$$

Taking into account the associate characteristic speeds, the corresponding reconstructions are

$$R_j^+(x_{j+\frac{1}{2}}, \bar{W}) = \bar{W}_j + \frac{\sigma_j^+}{2},$$

$$R_j^-(x_{j-\frac{1}{2}}, \bar{Z}) = \bar{Z}_j - \frac{\sigma_j^-}{2},$$

where $\sigma_j^+ = \partial_x W(x_j, \cdot) \Delta x + O(\Delta x^2)$ and $\sigma_j^- = \partial_x Z(x_j, \cdot) \Delta x + O(\Delta x^2)$ are obtained with the Van Leer slope limiter [3]. Using (4.9) to recover the original variables, we obtain the numerical fluxes

$$G_{j+\frac{1}{2}}(U) = \frac{1}{2c} (R_j^+(x_{j+\frac{1}{2}}, \bar{V} + A\bar{U}) - R_{j+1}^-(x_{j+\frac{1}{2}}, \bar{V} - A\bar{U})),$$

$$G_{j+\frac{1}{2}}(V) = \frac{1}{2} (R_j^+(x_{j+\frac{1}{2}}, \bar{V} + A\bar{U}) + R_{j+1}^-(x_{j+\frac{1}{2}}, \bar{V} - A\bar{U})).$$

Finally, the MUSCL scheme used here combines this spatial approximation with a second-order Runge–Kutta method [9], which is TVD, provided that the CFL condition $1/2$ is satisfied. Now, we can describe the full relaxation schemes used here. In the first case, we solve numerically the stiff ODE, with the above-mentioned implicit second-order Runge–Kutta method [4] (see also [5]) to obtain the relaxation (called relaxing in [4]) scheme

$$(4.11) \quad \begin{cases} \bar{U}_j^{n+\frac{1}{4}} = \bar{U}_j^n, \\ \bar{V}_j^{n+\frac{1}{4}} = \bar{V}_j^n - \frac{\Delta t}{\epsilon}(F(\bar{U}_j^{n+\frac{1}{4}}) - \bar{V}_j^{n+\frac{1}{4}}), \end{cases}$$

$$(4.12) \quad \begin{cases} \bar{U}_j^{n+\frac{2}{4}} = \bar{U}_j^{n+\frac{1}{4}} - \Delta t D_j^{conv} V^{n+\frac{1}{4}}, \\ \bar{V}_j^{n+\frac{2}{4}} = \bar{V}_j^{n+\frac{1}{4}} - \Delta t A^2 D_j^{conv} U^{n+\frac{1}{4}}, \end{cases}$$

$$(4.13) \quad \begin{cases} \bar{U}_j^{n+\frac{3}{4}} = \bar{U}_j^{n+\frac{2}{4}}, \\ \bar{V}_j^{n+\frac{3}{4}} = \bar{V}_j^{n+\frac{2}{4}} + \frac{2\Delta t}{\epsilon}(F(\bar{U}_j^{n+\frac{1}{4}}) - \bar{V}_j^{n+\frac{1}{4}}) + \frac{\Delta t}{\epsilon}(F(\bar{U}_j^{n+\frac{3}{4}}) - \bar{V}_j^{n+\frac{3}{4}}), \end{cases}$$

$$(4.14) \quad \begin{cases} \bar{U}_j^{n+\frac{4}{4}} = \bar{U}_j^{n+\frac{3}{4}} - \Delta t D_j^{conv} V^{n+\frac{3}{4}}, \\ \bar{V}_j^{n+\frac{4}{4}} = \bar{V}_j^{n+\frac{3}{4}} - \Delta t A^2 D_j^{conv} U^{n+\frac{3}{4}}, \end{cases}$$

$$(4.15) \quad \begin{cases} \bar{U}_j^{n+1} = \frac{1}{2}(\bar{U}_j^{n+\frac{4}{4}} + \bar{U}_j^n), \\ \bar{V}_j^{n+1} = \frac{1}{2}(\bar{V}_j^{n+\frac{4}{4}} + \bar{V}_j^n). \end{cases}$$

In the second case, we just replace steps (4.11) (resp., (4.13)) by imposing the equilibrium relation (4.16) (resp., (4.17)):

$$(4.16) \quad \bar{V}_j^{n+\frac{1}{4}} = F(\bar{U}_j^{n+\frac{1}{4}}),$$

$$(4.17) \quad \bar{V}_j^{n+\frac{3}{4}} = F(\bar{U}_j^{n+\frac{3}{4}}).$$

The resulting scheme (4.16), (4.12), (4.17), (4.14), (4.15) is called the *zero-relaxation scheme*.³ In the case of (2.1), where $U = (u, v)$, we have also considered a physically more natural relaxation system:

$$(4.18) \quad \begin{cases} \partial_t u - \partial_x v = 0, \\ \partial_t v - \partial_x (c^2 u + Y) = 0, \\ \partial_t Y = \frac{1}{\epsilon}(\sigma(u) - c^2 u - Y). \end{cases}$$

The adaptation to this case is straightforward. We just note that the subcharacteristic condition is still

$$(4.19) \quad c^2 \geq \sigma'(u).$$

Remark. As is well known, if we approximate the convective part (4.6) by the upwind scheme with a CFL = 1 and impose the equilibrium in (4.5) for the 4×4 system, then we just recover the Lax–Friedrichs scheme for the equilibrium system (4.1). We note that the three eigenvalues of (4.18) are $-c, 0, c$ and therefore are interlaced with those of (2.1) in the sense of Chen, Levermore, and Liu [14].

³This is also called a *relaxed scheme* in [4].

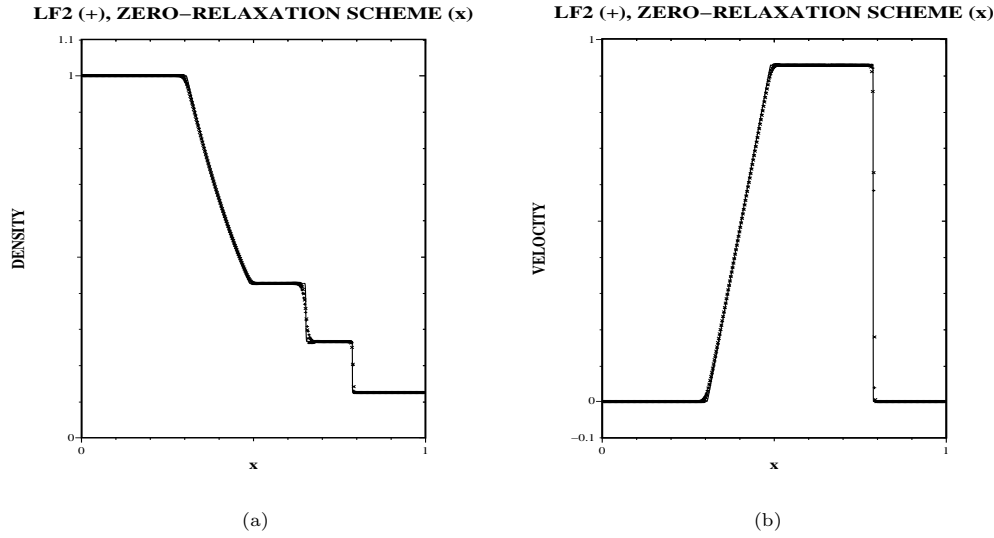


FIG. 5.1.

5. Numerical results. Before describing the results for the special p-system (2.1), we have first considered the test-case of a Sod shock tube for one-dimensional compressible Euler equations:

$$(5.1) \quad \begin{cases} \partial_t \rho + \partial_x m = 0, \\ \partial_t m + \partial_x \left(\frac{m^2}{\rho} + p \right) = 0, \\ \partial_t E + \partial_x \left(\frac{m}{\rho} (E + p) \right) = 0, \end{cases}$$

$$p = (\gamma - 1) \left(E - \frac{1}{2} \frac{m^2}{\rho} \right), \quad \gamma = 1.4.$$

5.1. The case of Sod's shock tube. On this problem, we have shown the results for the density and the velocity obtained with several schemes:

- (i) The second-order staggered Lax–Friedrichs scheme (3.7), (3.8) (plotted with +), and the zero-relaxation scheme (4.16), (4.12), (4.17), (4.14), (4.15) (plotted with ×) (see Figure 5.1);
- (ii) The relaxation scheme (4.11), (4.12), (4.12), (4.14), (4.15), with $\epsilon = 10^{-4}$ (plotted with +) and 10^{-8} (plotted with ×); see Figure 5.2.

The reference solution (plain line) has been obtained with the fourth-order WENO scheme with $\Delta x = .00025$. The numerical solution displayed with (+) or (×) is computed at time $t = .1644$, the space and time steps are $\Delta x = .0025$, $\Delta t = .0005565$, and the Riemann data are $(\rho, m, E)^- = (1, 0, 2.5)$, $(\rho, m, E)^+ = (.125, 0, .25)$.

We have compared these schemes more precisely. In Figure 5.3, we have simultaneously plotted the *differences* between the reference solution and

- (i) LF2 plotted with (+),
- (ii) the zero-relaxation plotted with (×).

In the same way, Figure 5.4 shows the *differences* between the zero-relaxation and

- (i) the $\epsilon = 10^{-4}$ case plotted with (+),
- (ii) the $\epsilon = 10^{-8}$ case plotted with (×).

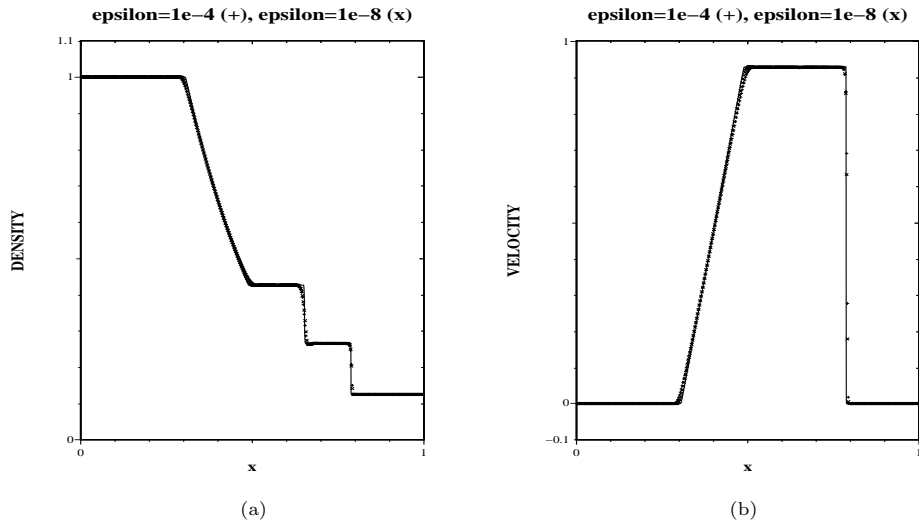


FIG. 5.2.

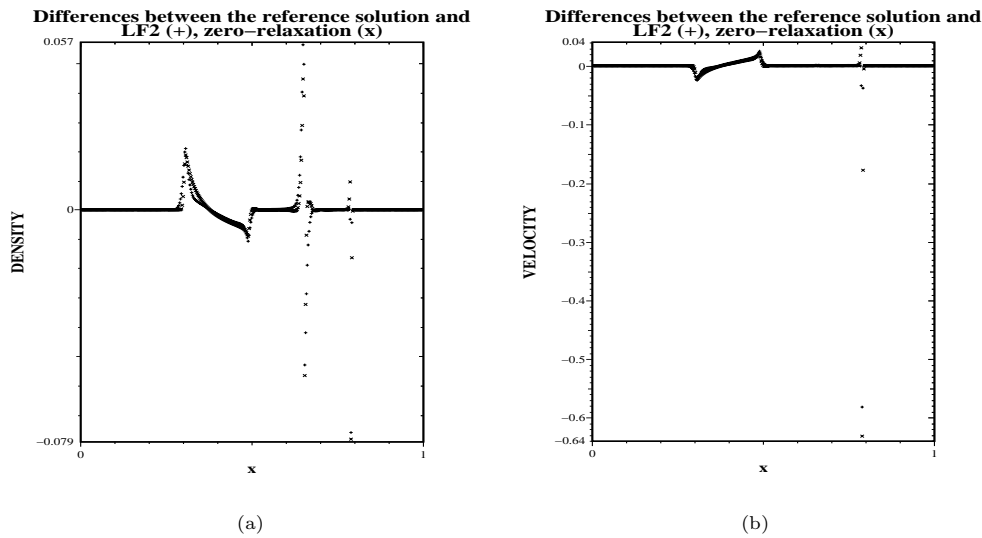


FIG. 5.3.

Comments.

1. The relaxation (“relaxing”) and the zero-relaxation (“relaxed”) schemes have been tested in [4] with the same matrix A^2 , with a CFL = 0.75 and $\Delta x = 0.005$ instead of CFL = 0.5 and $\Delta x = 0.0025$ here, which may explain why our numerical results are nicer.
2. All the schemes studied here give comparable results. We see in Figures 5.1 and 5.3 that the LF2 scheme produces a slightly sharper shock than the zero-relaxation (one grid point instead of three), but on the contrary the contact discontinuity and the rarefaction wave are slightly more spread out.
3. Not surprisingly, in Figures 5.2 and 5.4, the results of the zero-relaxation

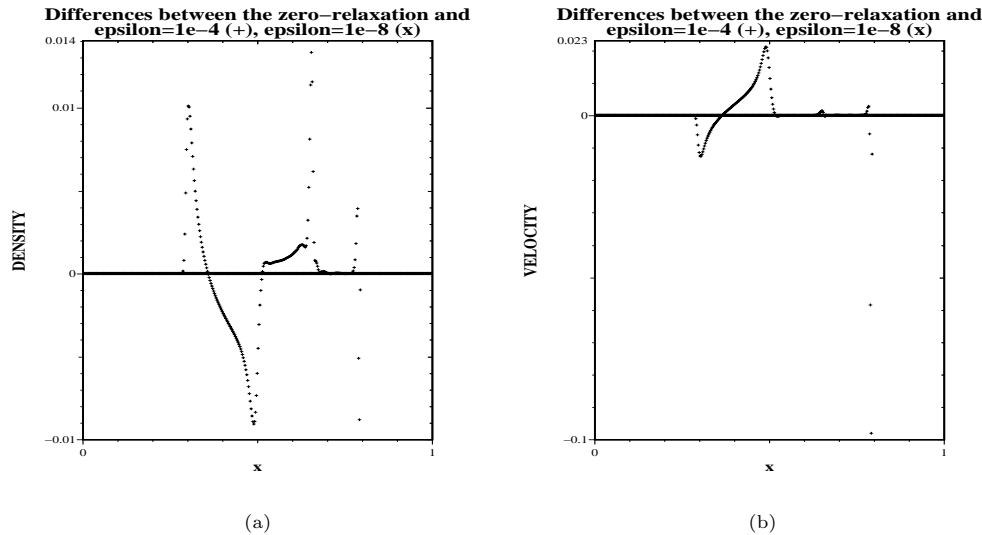


FIG. 5.4.

scheme are almost exactly the same—up to 10^{-6} —as in the case $\epsilon = 10^{-8}$. In fact, the curves are indistinguishable. On the other hand the waves are (slightly) more spread out in the $\epsilon = 10^{-4}$ case, with a maximal difference of 10^{-2} with the zero-relaxation case. We recall that $\Delta t \simeq 5.6 \cdot 10^{-4}$, so that in this case $\Delta t/\epsilon = 5.6 = O(1)$. In all cases the maximal difference is reached at the shock or at the contact discontinuity (except of course for the velocity and the pressure) but is also not negligible at the edges of the rarefaction wave (see Figures 5.3 and 5.4).

4. In the following, we will compare only the zero-relaxation and the second-order staggered Lax–Friedrichs scheme with the other high-order schemes.

5.2. The special p-system. We have considered the case where the parameters given in section 2 are $c_0 = 0.75$, $u_0 = 0.25$, $x_0 = 0.25$, $\lambda = 1$, $x_1 = 1$, $t_1 = 1$.

The initial data are alternately $N := (u_0, 0)$ and $S := (-u_0, 0)$. The space and time steps are $\Delta x = 2.10^{-3}$ and $\Delta t = 5.10^{-4}$; the CFL condition is $1/3$. The solution therefore consists of 4×4 basic patterns. See the graph of the strain-stress relation $\sigma(u)$ in Figure 5.5. We have considered

- (i) The second-order zero-relaxation scheme (4.16), (4.12), (4.17), (4.14), (4.15), either for the 4×4 system (4.2), (4.3) (see Figure 5.6) or for the physically more natural 3×3 system (4.18) (see Figure 5.7);
- (ii) The second-order staggered Lax–Friedrichs scheme (3.7), (3.8) (see Figure 5.8);
- (iii) The ENO schemes (3.6) of order 2 (see Figure 5.9) or of order 4 (see Figure 5.10);
- (iv) The WENO scheme of order 4 (see Figure 5.11).

In all the figures, the results are displayed at final time $t = 1$, and the u (resp., v) component is displayed in part (a) (resp., (b)). We have also displayed in Figures 5.13 and 5.14 the numerical results—only with the second-order zero-relaxation scheme—at time $t = 0.75$, which corresponds to the inflection point at $u = 0$; see Figure 5.5.

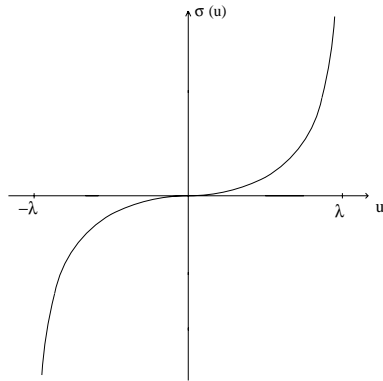


FIG. 5.5.

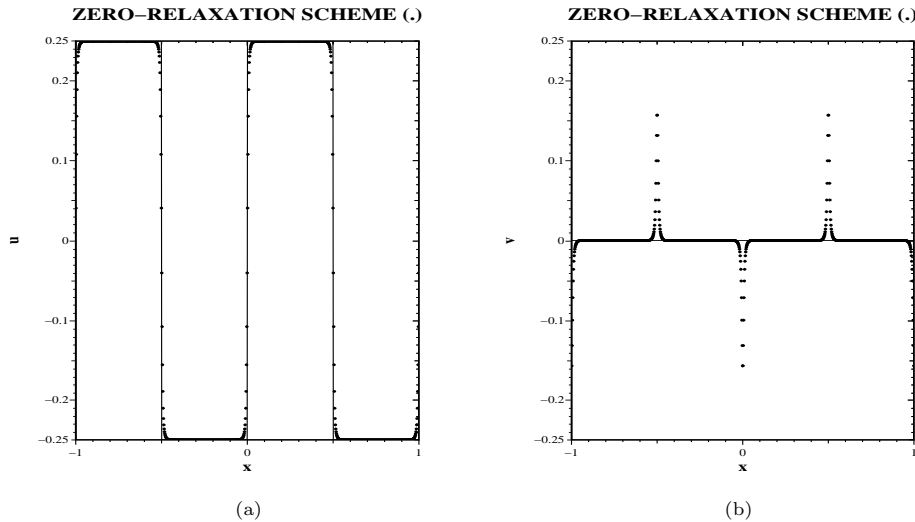


FIG. 5.6.

Comments. All the schemes are comparable—with sharper fronts for the fourth-order schemes—and give quite good results, apart from the numerical spikes. Those numerical spikes involve only the velocity v and the biggest ones are located near the centers of interacting compression waves, but there are also smaller ones at the inflection point $u = 0$, e.g., at $t = 0.75$ (see Figure 5.13(a)).

We first thought that this phenomenon was similar to the spikes produced by (first-order) Lax–Friedrichs scheme near a slowly moving shock [11]. In fact, this is not the case. The reason for those spikes is double. First, the exact solution itself presents big spikes in v , except *exactly* at time $t = 1$ (see Figure 2.2), and next, the numerical propagation speed is slightly smaller than the exact one. Therefore, the numerical solution depicted, for instance, in Figure 5.7, would be a better approximation of the exact solution at some time $t^* = 1 - O(\Delta t)$. Similarly, for instance, with the zero-relaxation scheme, the numerical results at time $t = 1 + 7\Delta t$ are much better (see Figure 5.12). The same phenomenon occurs near the inflection point at time $t = 0.75 + 6\Delta t$. See Figure 5.14(a). (We recall that $\Delta t = 5 \cdot 10^{-4}$.)

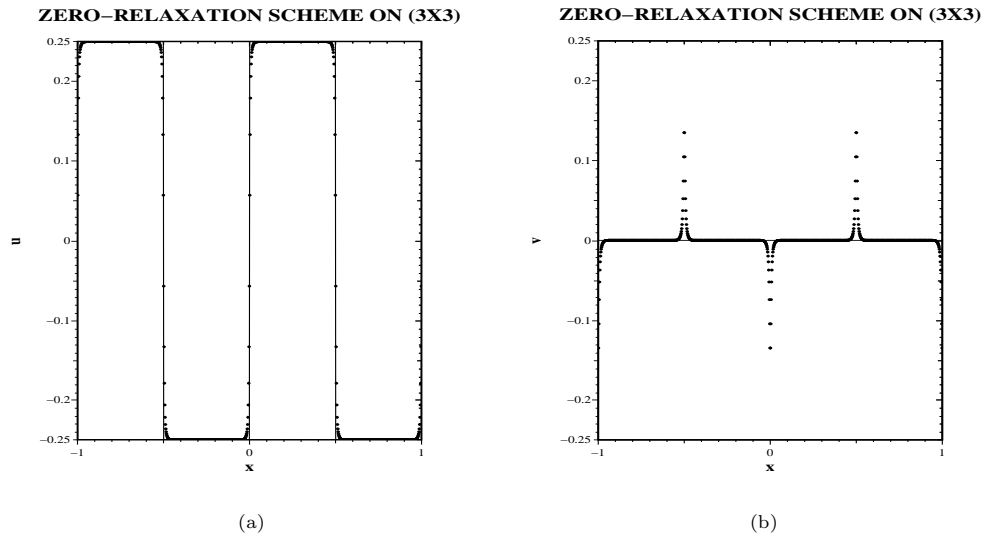


FIG. 5.7.

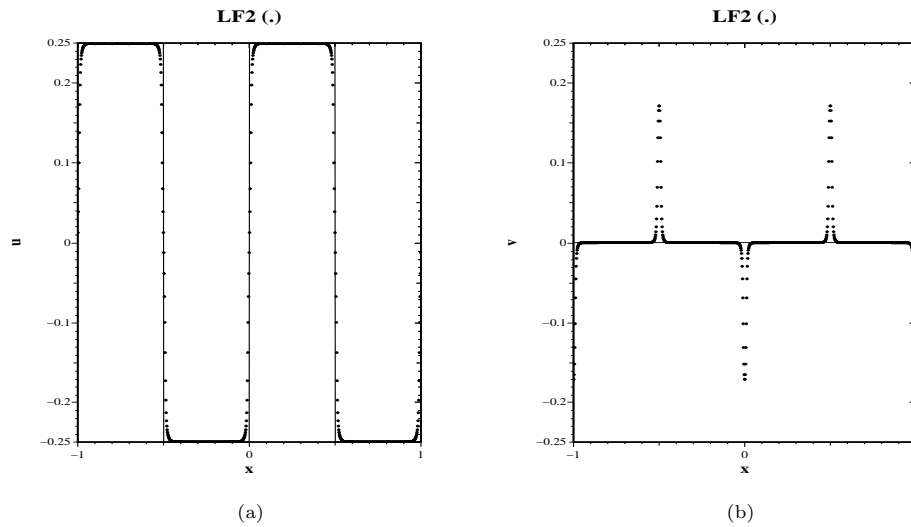


FIG. 5.8.

6. Conclusion. In this paper, we have considered and compared several classes of high-order finite volume schemes, first on Sod's shock tube for compressible Euler equations and then on a one-dimensional pathological example, where even the exact solution contains severe spikes due to the interaction of centered compression waves. All these schemes give comparable results and work rather well, considering the stiffness of the problem. The numerical spikes are essentially due to the fact that the numerical propagation speed is slightly smaller than the exact one, so that the numerical solution "is late." If the problem were linear, a classical Fourier analysis would probably explain this phenomenon.

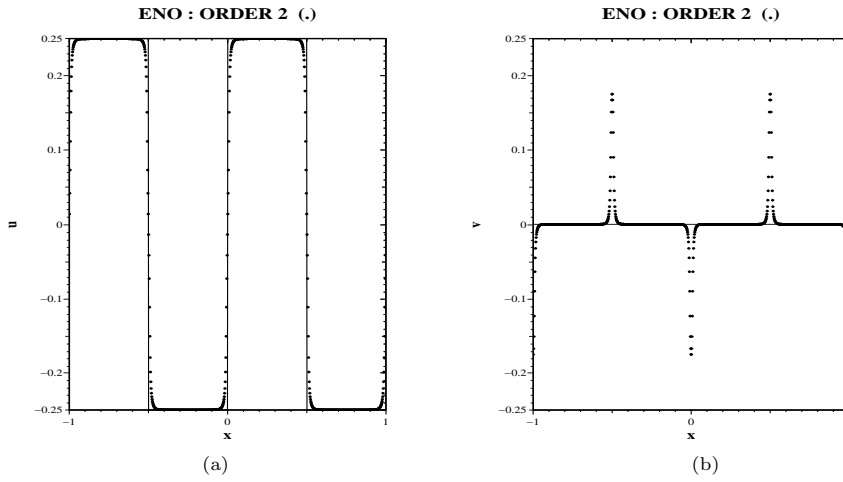


FIG. 5.9.

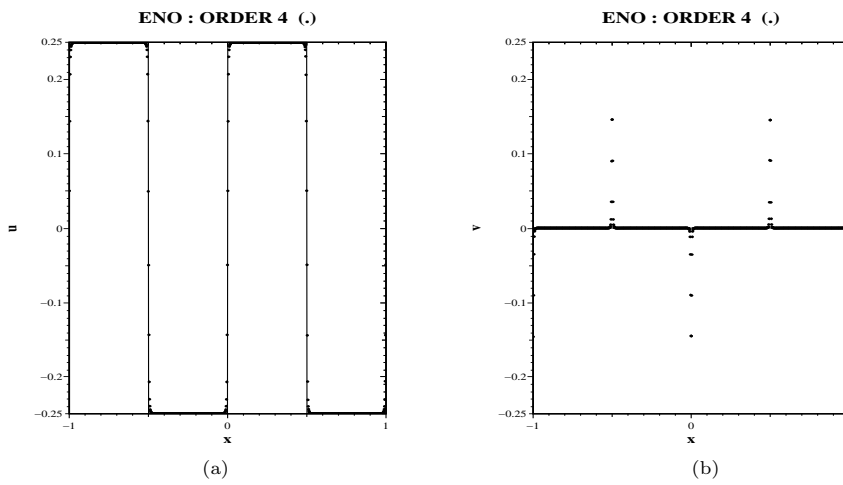


FIG. 5.10.

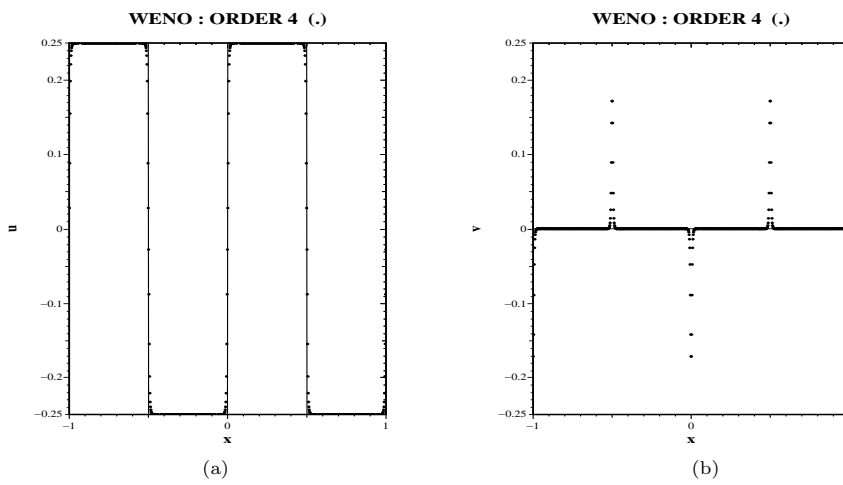


FIG. 5.11.

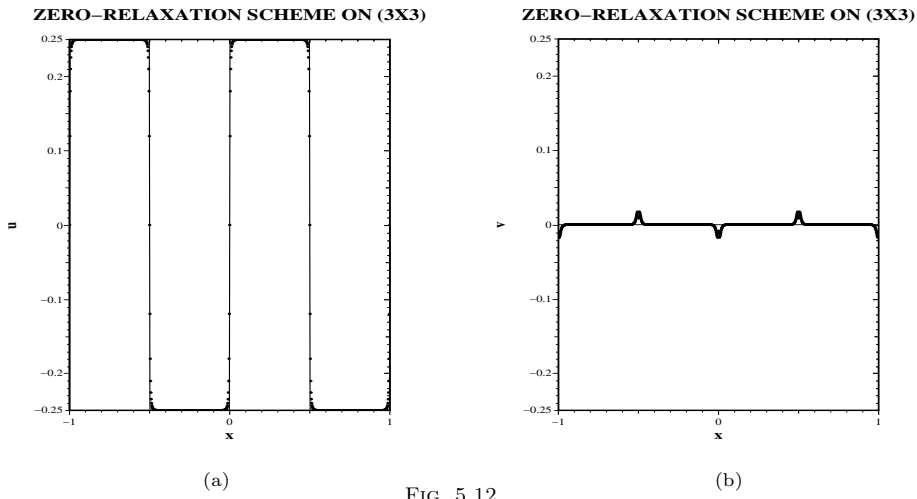


FIG. 5.12.

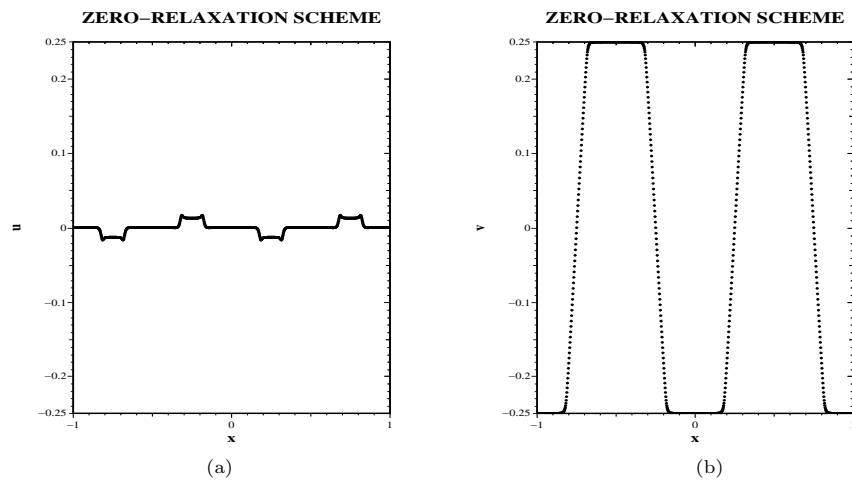


FIG. 5.13.

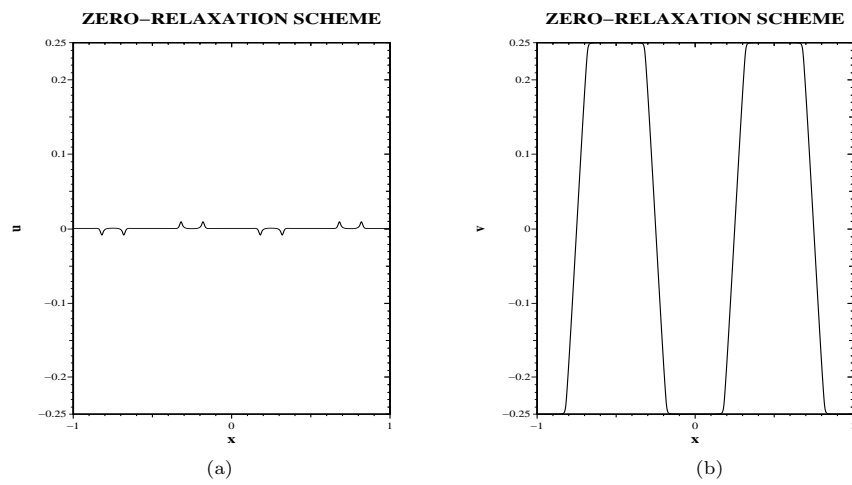


FIG. 5.14.

REFERENCES

- [1] J.M. GREENBERG AND M. RASCLE, *Time-periodic solutions to systems of conservation laws*, Arch. Rational Mech. Anal., 115 (1991), pp. 395–407.
- [2] J.M. GREENBERG AND R. PESZEK, *Time-periodic solutions to a class of quasilinear wave equations*, Arch. Rational Mech. Anal., 122 (1993), pp. 35–51.
- [3] P.K. SWEBY, *High resolution schemes using flux limiters for hyperbolic conservation laws*, SIAM J. Numer. Anal., 21 (1984), pp. 995–1011.
- [4] S. JIN AND Z. XIN, *The relaxing schemes for systems of conservation laws in arbitrary space dimensions*, Comm. Pure Appl. Math., 48 (1995), pp. 235–277.
- [5] R.E. CAFLISCH, S. JIN, AND G. RUSSO, *Uniformly accurate schemes for hyperbolic systems with relaxation*, SIAM J. Numer. Anal., 34 (1997), pp. 246–281.
- [6] H. NESSYAHU AND E. TADMOR, *Non-oscillatory central differencing for hyperbolic conservation laws*, J. Comput. Phys., 87 (1990), pp. 408–463.
- [7] A. HARTEN AND S. OSHER, *Uniformly high-order accurate nonoscillatory schemes, I*, SIAM J. Numer. Anal., 24 (1987), pp. 279–309.
- [8] A. HARTEN, S. OSHER, B. ENGQUIST, AND L. CHAKRAVARTHY, *Uniformly high order accurate essentially non-oscillatory schemes, III*, J. Comput. Phys., 71 (1987), pp. 231–303.
- [9] S. OSHER AND C.W. SHU, *Efficient implementation of ENO schemes, I*, J. Comput. Phys., 77 (1988), pp. 439–471.
- [10] X.D. LIU, S. OSHER, AND T. CHAN, *Weighted essentially non-oscillatory schemes*, J. Comput. Phys., 115 (1994), pp. 200–212.
- [11] S. JIN AND J.G. LIU, *The effects of numerical viscosities I: Slowly moving shocks*, J. Comput. Phys., 126 (1996), pp. 373–389.
- [12] R. DI PERNA, *Convergence of approximate solutions to conservation laws*, Arch. Rational Mech. Anal., 82 (1983), pp. 27–70.
- [13] T.P. LIU, *Hyperbolic conservation laws with relaxation*, Comm. Math. Phys., 108 (1987), pp. 153–175.
- [14] G.Q. CHEN, C.D. LEVERMORE, AND T.P. LIU, *Hyperbolic conservation laws with stiff relaxation terms and entropy*, Comm. Pure Appl. Math., 47 (1994), pp. 787–830.
- [15] G.B. WHITHAM, *Linear and Non Linear Waves*, John Wiley and Sons, New York, 1974.
- [16] D. SERRE, *Oscillations non linéaires des systèmes hyperboliques: Méthodes et résultats qualitatifs*, Ann. Inst. H. Poincaré Anal. Non Linéaire, 8 (1991), pp. 351–417.
- [17] D. SERRE, *Oscillations non-linéaires de haute fréquence, Dim = 1*, Nonlinear PDEs and Their Applications, Collège de France Seminar XII, Longman Press, London, 1994.
- [18] C. CERCIGNANI, *The Boltzmann Equation and Its Applications*, Springer-Verlag, New York, 1988.